

## Original Article

# Antimicrobial & anticancer activities of extracellular silver nanoparticles biosynthesised by *Haloferax* sp SNP6

Hend M. Tag<sup>1</sup>, Naglaa Elshafey<sup>3</sup>, Muhammad A. Abuelmagd<sup>4,†</sup>, Ragaa A. Hamouda<sup>2,5,#</sup> & Nashwa Hagagy<sup>2,6</sup>

<sup>1</sup>Department of Nursing, College of Applied Medical Sciences, University of Jeddah, <sup>2</sup>Department of Biology, College of Sciences and Arts Khulis, University of Jeddah, Jeddah, Saudi Arabia, <sup>3</sup>Botany and Microbiology Department, Faculty of Science, Arish University, Al-Arish, <sup>4</sup>Department of Botany, Faculty of Science, Mansoura University, Mansoura, <sup>5</sup>Microbial Biotechnology Department, Genetic Engineering and Biotechnology Research Institute, University of Sadat City, Sadat City & <sup>6</sup>Botany and Microbiology Department, Faculty of Sciences, Suez Canal University, Ismailia, Egypt

Received August 11, 2024; Accepted May 26, 2025; Published September 16, 2025

**Background & objectives:** Nanotechnology-based therapeutics offer promising strategies for treating infectious diseases and cancer. Silver nanoparticles (AgNPs), in particular, exhibit strong antimicrobial and anticancer properties. Biologically synthesized AgNPs are preferred for their safety and environmental compatibility. *Haloferax* species, known for their extremophilic nature, present a novel biosynthetic platform. This study aimed to evaluate the antimicrobial and anticancer activities of extracellular AgNPs biosynthesized by *Haloferax* sp SNP6 and assess their effects on selected human cancer cell lines.

**Methods:** Initially, the extracellular silver NPs were biosynthesized using *Haloferax* sp SNP6. These nanoparticles were then characterized using several techniques, including X-ray diffraction (XRD), transmission electron microscopy (TEM), Fourier-transform infrared spectroscopy (FTIR), and UV spectroscopy. The purpose of these analyses was to confirm the formation, size, shape, and functional groups associated with the Ag-NPs. Their antimicrobial efficacy was tested against several pathogenic bacteria and fungi using standard microbiological methods. The cytotoxic effects were assessed on human cancer cell lines (breast and cervical) and compared with those on a non-cancerous human cell line.

**Results:** The biogenic Ag-NPs via *Haloferax* sp exhibited significant antimicrobial activity against *Escherichia coli* (ATCC 8739), *Bacillus subtilis* (ATCC 6633), *Pseudomonas aeruginosa* (ATCC 90274), *Staphylococcus aureus* (ATCC 6538), *Aspergillus niger*, and *Candida albicans* (ATCC 10221), which

Nanobiotechnology is recognised as a significant advancement in medicine, encompassing the synthesis

and application of various nanoparticles (NPs) for disease treatment and precise drug delivery. The

Present address: <sup>†</sup>Faculty of Pharmacy, Mansoura National University, Gamasa, Egypt

<sup>#</sup>Department of Applied Radiologic Technology, College of Applied Medical Sciences, University of Jeddah, Jeddah, Saudi Arabia

possessed clear zones of  $18\pm 1.1$ ,  $28\pm 1.7$ ,  $24\pm 1.3$ ,  $18\pm 1.2$ ,  $0$ , and  $27\pm 2.0$ , respectively. The biogenic Ag-NPs via *Haloferax* sp (*Hal*-AgNPs) demonstrated potent cytotoxic effects on cancer cell lines, with lower  $IC_{50}$  values indicating higher efficacy and minimal toxicity toward non-cancerous cells. The NPs presented a unique combination of size, stability, and surface characteristics, contributing to their biological activities. The TEM image of *Hal*-AgNPs demonstrated semi-spherical-shaped particles ranging from 2 to 14 nm, and XRD proved that the *Hal*-AgNPs are crystalline.

**Interpretation & conclusions:** The observed findings of this study suggest a dual functionality of the biosynthesized silver nanoparticles (*Hal*-AgNPs) as antimicrobials and anticancer agents highlighting their potential as therapeutic agents, especially in treating drug-resistant infections and cancer.

**Key words** Anticancer - antimicrobial activity - cytotoxicity - *Haloferax* sp - silver nanoparticles

production of NPs by organisms is crucial due to their simplicity in manufacturing, sustainability, and capacity to be absorbed by the body. Green nanotechnology involves the synthesis of stable NPs coated with metabolites derived from microorganisms or plants<sup>1</sup>. Nanomaterials are particularly valuable in combating infections and cancer cells generated by drug-resistant bacteria. The medical industry is increasingly studying silver NPs (AgNPs) due to their distinctive physical, chemical, and optical characteristics<sup>2</sup>. The potential cooperation between the pharmacological effectiveness of anticancer medications and the intrinsic anticancer properties of Ag-NPs presents new therapeutic approaches for treating tumours that exhibit resistance to traditional chemotherapy or radiotherapy. Ag-NPs represent a promising approach to cancer treatment due to their ability to deliver anticancer drugs to tumours. Recent research has demonstrated that Ag-NPs possess inherent antibacterial and anticancer capabilities through various pathways<sup>3</sup>. Cancer remains the most common cause of mortality worldwide, impacting countries with both high and medium incomes<sup>4</sup>. The top five cancers with the most significant death rates globally are lung cancer (18%), colorectal cancer (9.4%), liver cancer (8.3%), stomach cancer (7.7%), and breast cancer (6.9%), according to data from the Global Cancer Observatory (GLOBOCAN)<sup>5</sup>. The prevalence of cervical cancer is the fourth highest among females globally<sup>6</sup>, and it ranks as the second leading cause of cancer-related deaths among women aged 20 to 39 yr in the United States<sup>5</sup>. The current emphasis in nanotechnology studies depends on developing innovative, powerful, and precise anticancer medications<sup>7</sup>. AgNPs have been extensively studied across various scientific fields<sup>8</sup>. Notably, AgNPs exhibit potent antimicrobial properties and disrupt microbial development through multiple mechanisms, including damage to the cell wall and

interference with metabolic processes, as reported by Xu *et al*<sup>9</sup>. The current study demonstrates the extracellular production of Ag NPs by an unidentified *Haloarchaea* species, specifically *Haloferax* sp strain SNP6. The biosynthesised *Hal*-AgNPs were characterised using UV spectroscopy, TEM, FTIR, and XRD. The primary goal of this study was to investigate the potential application of environmentally friendly AgNPs (*Hal*-AgNPs) generated by *Haloferax* sp strain SNP6 through biological synthesis, focusing on their antimicrobial properties, haemolytic activity, and cytotoxic effects on human cancer cells, specifically breast and cervical cancer cells.

## Materials & Methods

The biosynthesis and antimicrobial experiments were conducted at the department of Biology, College of Sciences and Arts - Khulis, University of Jeddah, while the cancer cell line assays were carried out at the Faculty of Science, Mansoura University, Egypt. The research protocol involving the biosynthesis of *Hal*-AgNPs and their evaluation on human cancer cell lines was approved by the URAF-IACUC at Cairo University. The study was approved by the Institutional Animal care and use committee before starting the study. The study adhered to institutional and international ethical standards, including the Declaration of Helsinki, for research involving human-derived cell lines.

**Sampling and site description:** Samples of brine and sediment were sampled from a solar salt pan located on Jeddah's southern beach (coordinates:  $21^{\circ}10'16.04''N$ ,  $39^{\circ}11'5.94''E$ ), Saudi Arabia, from October 2023 to April 2024. Initial microbiological isolation and primary screening were conducted.

**Isolation and cultivation conditions:** *Haloarchaea* were isolated from brine and sediment samples using

the method as described previously<sup>10</sup>. This method involves using NTYE (25% NaCl, 2% MgSO<sub>4</sub>.7H<sub>2</sub>O, 0.5% KCl, 0.5% tryptone, 0.3% yeast extract, and 2% agar). The pure strains were acquired by repeatedly culturing and preserving them on NTYE.

*Screening for Haloarchaeal strains resistant to silver:* Following a two wk incubation period at 40°C, five distinct *Haloarchaeal* isolates were successfully obtained<sup>10</sup>. The isolates' ability to thrive in AgNO<sub>3</sub> concentrations from 0.05 to 1 mM was examined. The cell culture was analysed using a UV-spectrophotometer (UV-2600 Series, SHIMADZU) at 600 nm. The medium lacking AgNO<sub>3</sub> served as a negative control, while non-inoculated media with AgNO<sub>3</sub> served as a positive control.

*Extracellular synthesis of silver nitrate NPs:* The chosen *Haloarchaeal* strain SNP6 was cultured using the NTYE, supplemented with 0.5 mM AgNO<sub>3</sub>. The transition of colour from red to brown<sup>11</sup> evidenced the visual observation of NP biosynthesis. The supernatant with AgNPs was concentrated by spinning through an Ultra-15 Centrifugal Millipore membrane (Amicon) with a 3,000 Da cutoff for 10 min at 4°C at 14,000 rpm. To collect the NPs, they were dried on a glass slide, rinsed with one per cent glacial acetic acid, and scraped into a powder.

*Identification of the isolates:* The *Haloferax* sp strain SNP6 genomic DNA was isolated using a modified method<sup>12</sup>. The 16S rRNA gene was amplified utilising universal primers specific to *Archaea* (Invitrogen, USA): 5'-ATT CCG GTT GAT CCT GCC GG-3' (positions 6-25) and 5'-AGG AGG TGA TCC AGC CGC AG-3' (positions 1540-1521)<sup>13</sup>. PCR was performed under standard thermal cycling conditions: 30 cycles of 95°C for 5 min (pre-denaturation), 94°C for 1 min (denaturation), 60°C for 1 min (annealing), and 72°C for 1.5 min (extension), followed by a final elongation at 72°C for 10 min. PCR products were sequenced by MacroGen (Korea). Strain identification was done using NCBI BLAST, and phylogenetic analysis was conducted using MEGA11 software.

*Characterisation of extracellular synthesised AgNPs:* The UV-2600 Series spectrophotometer (SHIMADZU) was employed to determine the extinction coefficient of the colloidal solution of *Hal*-AgNPs. Transmission electron microscopy (TEM) was used to assess the morphology and size of *Hal*-AgNPs, utilising the HF-3300 model from Hitachi High-Tech Canada, Inc. A

second analysis of the *Hal*-AgNP size distributions was conducted with ImageJ, a free programme (Version 1.53d) downloaded from the NIH website (<http://rsb.info.nih.gov/ij>). A Malvern analytical X-ray diffractometer (XRD) was employed for structural characterisation. The active groups were identified using a Perkin-Elmer Spectrum GX spectrometer and Fourier-transform infrared spectroscopy (FTIR).

*Antimicrobial activity of Hal-AgNPs:* The antimicrobial activity of *Hal*-AgNPs was assessed using the agar well-diffusion method by the guidelines outlined by Espinel-Ingroff *et al*<sup>14</sup>. This method was employed against six microbial strains: *Escherichia coli* (ATCC 8739), *Staphylococcus aureus* (ATCC 6538), *Bacillus subtilis* (ATCC 6633), *Pseudomonas aeruginosa* (ATCC 90274), *Aspergillus niger*, and *Candida albicans* (ATCC 10221). Wells were loaded with 50 µL of *Hal*-AgNPs, with gentamicin as the positive control for bacterial strains and fluconazole for fungal strains. All experiments were conducted in triplicate to ensure data accuracy and reproducibility.

*Determination of Minimal-Inhibitory-Concentration (MIC):* MIC of *Hal*-AgNPs was assessed for microbial strains showing positive results. *Hal*-AgNPs were diluted to concentrations (31.25, 62.5, 125, 250, 500, and 1000 µg/mL) and mixed with fresh microbial colonies (10<sup>6</sup> to 10<sup>8</sup> CFU/mL). The tubes were incubated for 24 h at 37°C with a control. The MIC endpoint was determined as the lowest concentration showing no visible growth. Tube turbidity was recorded before and after incubation to validate the MIC value.

*Haemolytic action of Hal-AgNPs:* Haemolytic activity of *Hal*-AgNPs was assessed by incubating human red blood cells (RBCs) from healthy donors with NP concentrations ranging from 50 to 1000 µg/mL. RBCs were washed and resuspended in phosphate buffer (pH 7.4), mixed with *Hal*-AgNPs, and incubated at 37°C for 1 h. Following centrifugation, the absorbance of the supernatant was measured at 541 nm. Haemolysis percentage was calculated using the formula:

$$\text{Haemolysis (\%)} = \frac{[(\text{Abs sample} - \text{Abs blank}) / \text{Abs positive control}] \times 100}{100}$$

Deionised water and PBS were used as positive and negative controls, respectively.

*Cytotoxicity of Hal-AgNPs on cancer cells:* The cytotoxicity of *Hal*-AgNPs was evaluated against human breast and cervical cancer cell lines, as well as

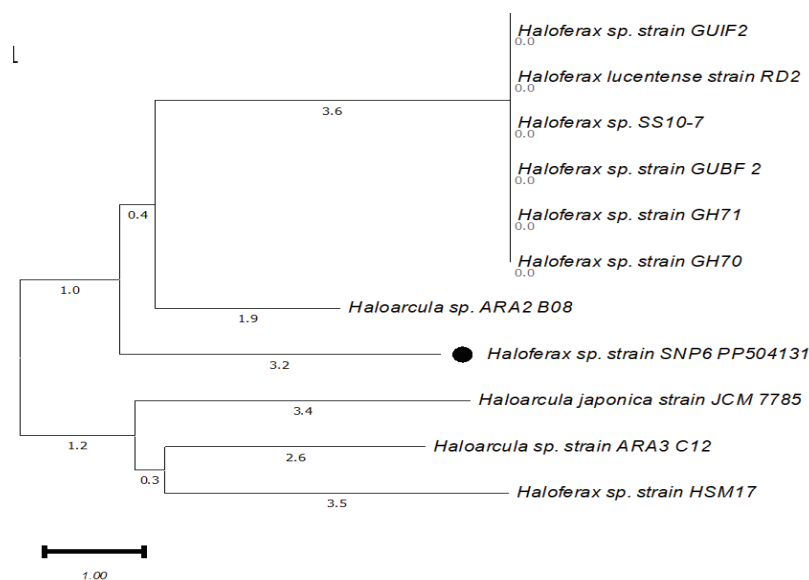


**Fig. 1.** Neighbour-Joining phylogenetic tree was constructed using 16S rRNA gene sequences to illustrate the relationship between *Haloferax* sp strain SNP6 and closely related taxa obtained from the NCBI database. The tree was generated using MEGA X software (Version 10.1.8). The scale bar represents a rate of 1 substitutions per nucleotide location.

non-cancerous Wi38 cells, in accordance with Hon *et al*<sup>5</sup>. Cells were cultured and treated with serial dilutions of *Hal*-AgNPs prepared in RPMI medium with 2 per cent serum. Following incubation, cell viability was assessed using the MTT assay. Absorbance was measured spectrophotometrically, and cytotoxic effects were quantified by comparing the treated and control. IC<sub>50</sub> values were calculated to determine the inhibitory concentration of *Hal*-AgNPs.

**Statistical analysis:** This study evaluated the biological activities of extracellular *Hal*-AgNPs strain SNP6 using two-tailed Independent Samples t-tests, conducted via SPSS (Version 26.0, IBM Corp.). Cytotoxicity was assessed on human cancer cell lines, compared with non-cancerous Wi38 fibroblasts. The two-tailed approach was employed to detect differences in either direction (increase or decrease) in cell viability and bacterial growth inhibition between the treatment and control groups, with *P* values of < 0.05 considered statistically significant. Data were expressed as mean±standard deviation (SD).

## Results

**Biosynthesis of extracellular AgNPs:** The nanoparticle formation is typically indicated based on monitoring the colour change following which the synthesis is confirmed. In this study, after incubating the culture supernatant of *Haloferax* sp strain SNP6 with AgNO<sub>3</sub>

(0.5 mM) at 37°C for one week, the colour changed from orange-red to brown-black. This change occurred when secondary metabolites from *Haloferax* sp strain SNP6 were mixed with a solution of silver nitrate. The control (culture media without AgNO<sub>3</sub>) showed no colour change. The existence of a brown colour demonstrated the Ag NPs formation.

**Archaeal strain identification:** The 16S rRNA gene sequencing examination showed that the archaeal strain belongs to the genus *Haloferax* and is more specifically selected as *Haloferax* sp. The sequence analysis reveals a similarity of approximately 90 per cent with known sequences. The 16S rRNA gene sequences for this *Haloarchaea* strain have been formally deposited in GenBank databases and are recorded with the accession number PP504131 (Fig. 1).

**Characterisation of synthesised Ag NPs:** The biosynthesised *Hal*-AgNPs exhibited semi-spherical morphology with sizes ranging from 2 to 14 nm, as observed by TEM, and were embedded in organic sheaths (Fig. 2). FTIR analysis revealed prominent absorption bands at 3453, 1634, 1111, and 603 cm<sup>-1</sup>, indicating the presence of functional groups that enhance nanoparticle stability. XRD analysis showed distinct peaks at 37.85°, 41.13°, 61.49°, and 74.23°, corresponding to the (111, 200, 220, and 311) planes, respectively, confirming the crystalline nature of the *Hal*-AgNPs (Fig. 3).

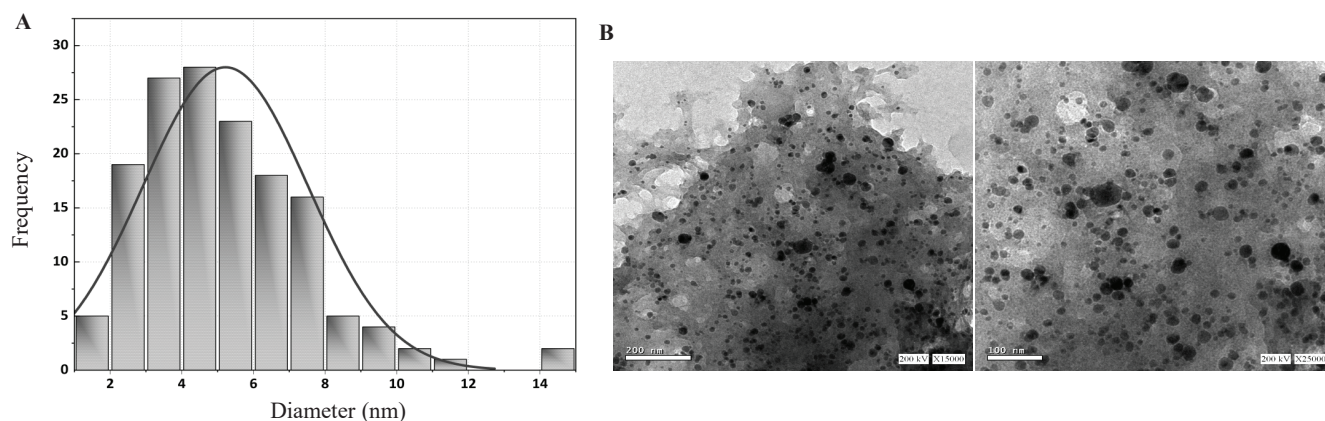


**Fig. 2.** (A) The histogram illustrates the distribution of particle diameter sizes of the *Hal*-AgNPs, which were determined through analysis of TEM images. The red line represents a Gaussian distribution function. (B) TEM images of *Hal*-AgNPs (scale bar = 100 nm).

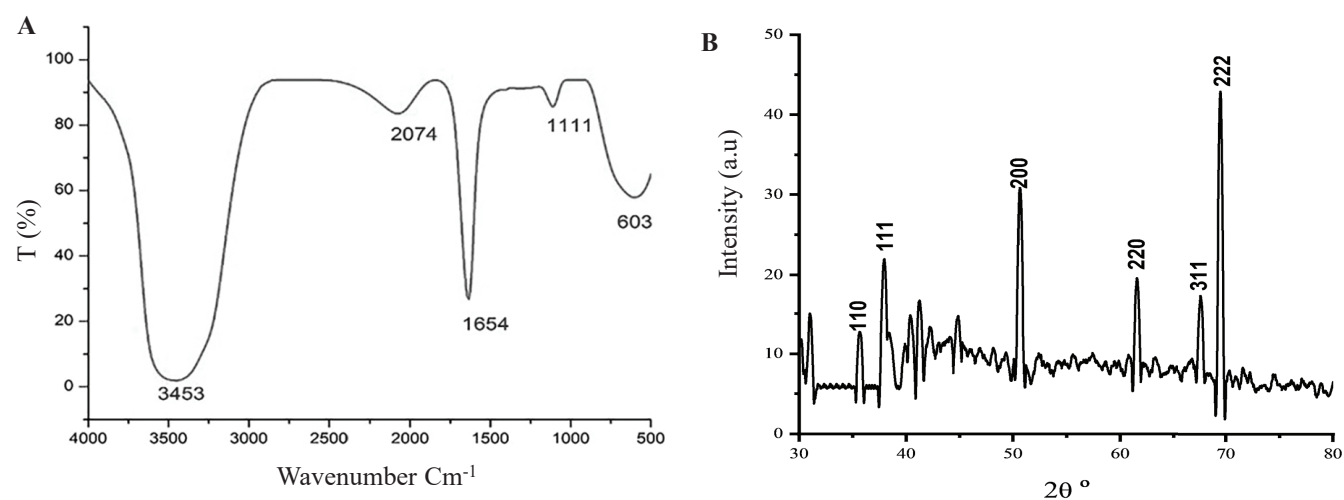


**Fig. 3.** (A) FTIR spectrum of *Hal*-AgNPs strain SNP6. (B) XRD AgNPs *Hal*-AgNPs strain SNP6.

**Antimicrobial activity of Hal-AgNPs:** Figure 4 shows a comparative analysis using an independent t-test to assess the antimicrobial efficacy of *Hal*-AgNPs and the standard drug against six pathogenic microbial strains. The results suggest that the antimicrobial efficacy of *Hal*-AgNPs closely resembles that of the reference medication. Regarding *B. subtilis*, the average inhibition zone for *Hal*-AgNPs ( $28 \pm 1.7$  mm) was slightly more significant than that for gentamicin ( $26 \pm 1.3$  mm). *S. aureus* exhibited similar inhibition zones for *Hal*-AgNPs ( $18 \pm 1.2$  mm) and gentamicin ( $16 \pm 1.0$  mm). *P. aeruginosa* exhibited a larger average inhibitory zone for *Hal*-AgNPs ( $24 \pm 1.5$  mm) than gentamicin ( $23 \pm 1.2$  mm). *E. coli* showed similar inhibitory zones for *Hal*-AgNPs ( $18 \pm 1.1$  mm) and gentamicin ( $17.0 \pm 1.2$  mm). *C. albicans* showed a somewhat larger zone of inhibition when exposed to *Hal*-AgNPs ( $27 \pm 2$  mm) compared to Fluconazole ( $25 \pm 1.1$  mm). Additionally, *A. niger* did

not display any activity towards *Hal*-AgNPs (NA), whereas Fluconazole demonstrated a mean inhibition zone of  $17 \pm 0.9$ . The MIC was utilised to evaluate the growth inhibitory effect of *Hal*-AgNPs against both bacterial and fungal species (Fig. 5). MIC values of *Hal*-AgNPs were recorded as 250, 62.5, 125, and 500  $\mu\text{g}/\text{mL}$  for *E. coli*, *B. subtilis*, *P. aeruginosa*, *S. aureus*, and *C. albicans*, respectively.

The cytotoxicity of extracellular *Hal*-AgNPs produced by *Haloferax* sp strain SNP6 was assessed by evaluating their haemolytic activity on RBC at different doses. The findings revealed a direct correlation between the dosage and the level of haemolytic activity, with the highest concentration of 1000  $\mu\text{g}/\text{mL}$  resulting in 4.5 per cent haemolysis. *Hal*-AgNPs demonstrated minimal haemolytic activity across all tested concentrations, with haemolysis consistently below 5 per cent. Notably, no haemolysis was observed

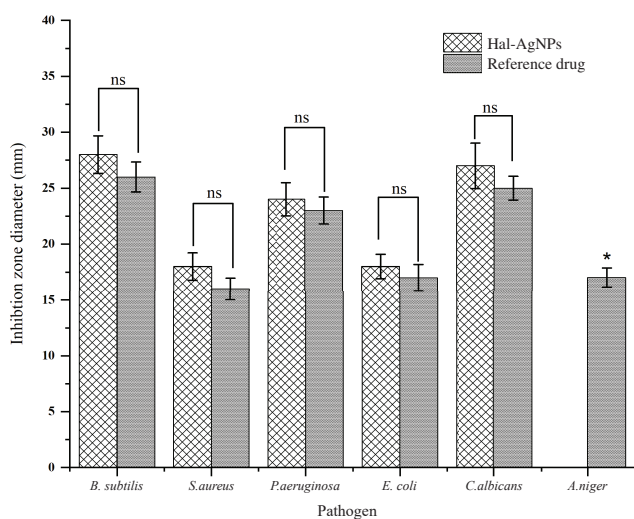


**Fig. 4.** Antimicrobial activity of *Hal-AgNPs* against pathogenic microbial strains.

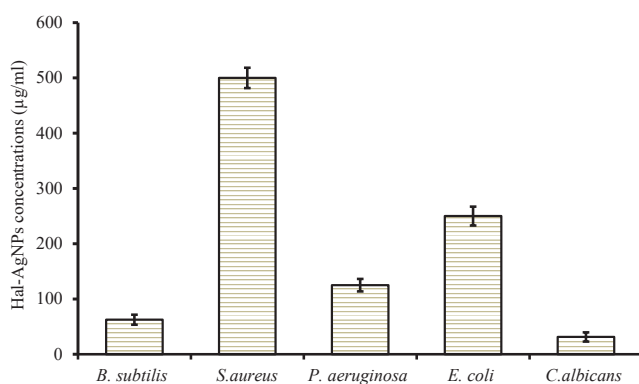


**Fig. 5.** MIC values for *Hal-AgNPs* against pathogenic microorganisms.

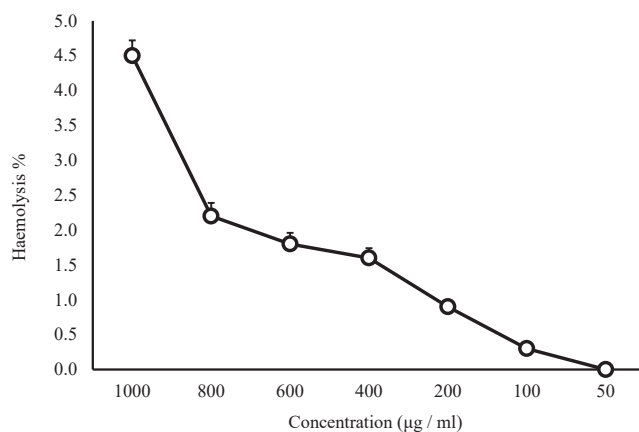


**Fig. 6.** Haemolytic action of *Hal-AgNPs*.

at 50 µg/mL, and only 2.2 per cent at the highest dose (800 µg/mL), indicating low cytotoxicity and good biocompatibility (Fig. 6).

The cytotoxic effects of *Hal-AgNPs* on various human cell lines, revealed distinct sensitivity patterns across cancerous and non-cancerous cells (Fig. 7). For cancer cell lines, MDA-MB231 and Mcf7 showed a high level of sensitivity to *Hal-AgNPs*, with  $IC_{50}$  values determined at  $113.3 \mu\text{g/mL} \pm 0.59$  and  $79.1 \mu\text{g/mL} \pm 0.9$ , respectively. This indicated a potent cytotoxic effect of *Hal-AgNPs* at relatively low concentrations. Similarly, the HELA cell line (cervical cancer) exhibited significant sensitivity, with an  $IC_{50}$  of  $83.56 \mu\text{g/mL} \pm 1.2$ . Conversely, the non-cancerous human cell line Wi38 demonstrated considerably higher NP resistance, with an  $IC_{50}$  value of  $218.1 \mu\text{g/mL} \pm 3.5$  suggesting that *Hal-AgNPs* have lower toxicity towards normal cells at the tested concentrations. The order of sensitivity, from most to least affected, was observed as follows: Mcf7 > HELA > MDA-MB231, with non-cancerous Wi38 cells showing the least sensitivity.

## Discussion

*Haloarchaea* have  $\gamma$ -glutamylcysteine ( $\gamma$ -GC), maintaining cell stability through its thiol group, which chelates harmful metal ions<sup>10</sup>. We hypothesised that *Haloferax* sp SNP6 may utilise similar mechanisms to resist heavy metals, making its production of extracellular AgNPs (*Hal-AgNPs*) significant for nanobiotechnology. Previous studies reported AgNPs biosynthesis from halophilic strains and showed how metabolites like carotenoids, biopolymers, bacteriorhodopsin, and enzymes reduce silver cations ( $\text{Ag}^+$ ) to zero-charged ones ( $\text{Ag}^0$ )<sup>16</sup>. TEM examination from the current study revealed that the biosynthesised *Hal-AgNPs* were semi-spherical in shape with particle sizes ranging from 2 to 14 nm. The TEM graphs also showed that these nanoparticles were surrounded by organic sheaths, likely composed of residual cellular polysaccharides, acting as dual-function reducing and stabilising agents<sup>17</sup>. These coatings and sheaths act as dual-function reducing and stabilising agents for *Hal-AgNPs*<sup>18,19</sup>.

The presence of amino, carbonyl, and hydroxyl groups in the FTIR pattern can indicate EPS/protein coating onto AgNPs, affecting NP stabilisation in the culture system<sup>20</sup>. A strong, broad band centred at  $3453 \text{ cm}^{-1}$  is typically attributed to the O-H stretching vibration of hydrogen-bonded hydroxyl groups in alcohols or phenols<sup>21</sup>. This broadening indicates intermolecular hydrogen bonding in polysaccharides or polyols linked to bioreduction and capping of NPs. An absorption peak at  $1634 \text{ cm}^{-1}$  corresponds to N-H bending vibrations or

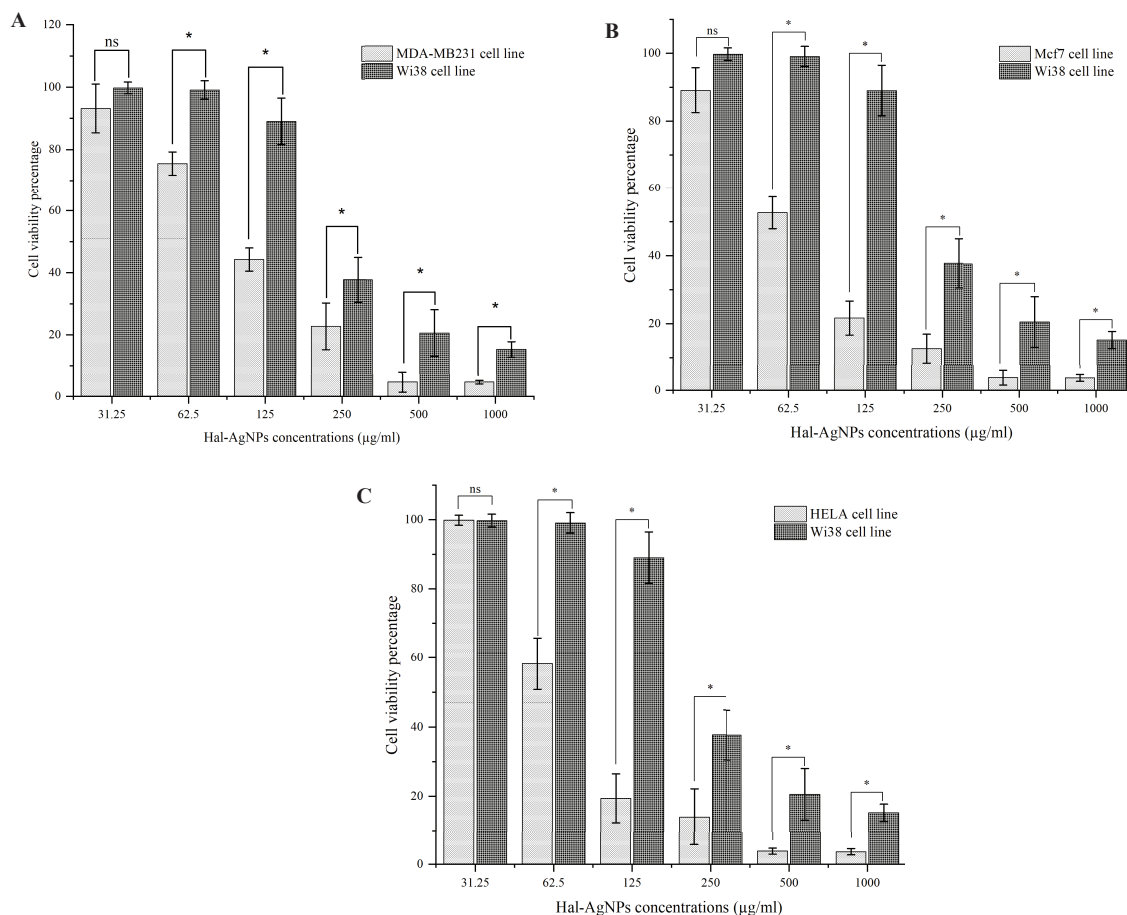


**Fig. 7.** Cell viability percentage of (A) MDA-MB-231, (B) MCF7, and (C) HeLa cells compared with Wi38 Cell Line (non-cancerous human cell line), treated with *Hal*-AgNPs.

C=O stretching from amide connections, suggesting peptide bonds or amino acid residues. These features are typical of proteinaceous materials used as biocapping agents in NP manufacturing<sup>22</sup>. A broad peak at 603  $\text{cm}^{-1}$  suggests phosphate-containing biomolecules, attributed to P-O bending or stretching modes, known for creating surface complexes with metal ions and stabilising NPs. Previous studies on *Haloferox* sp strain NRS1 confirm this through similar FTIR features and XRD patterns matching crystalline planes (111), (200), (220), and (311), verifying the metallic character and face-centred cubic structure of biosynthesised AgNPs<sup>11</sup>. This interaction enables proteins to act as capping agents, preventing NP aggregation through steric and electrostatic stabilisation, thus enhancing colloidal stability. This aligns with previous findings that biomolecules both stabilise the nanostructures and reduce metal-ions<sup>23</sup>.

Ag NPs' bactericidal effect occurs through interaction with bacterial cell walls, compromising membrane integrity and causing cell death<sup>17</sup>. Their

multifunctionality enables use in coatings, fabrics, and medical devices beyond pharmaceuticals<sup>19</sup>. Indeed, synthesised AgNPs have a more decisive antimicrobial action against Gram-negative bacteria than Gram-positive ones<sup>24</sup>. This effectiveness may be because of the nature of the bacterial cell wall, which is composed of a dense layer of peptidoglycan in Gram-positive bacteria, comparable to Gram-negative bacteria<sup>25</sup>. AgNPs interact with bacterial cell wall sulphur-containing proteins, inducing permanent changes that deactivate them and disrupt lipid bilayer integrity<sup>26</sup>. The smaller size of AgNPs enhances the penetration power, accumulation, and interaction of silver particles with fungal cell membranes and, consequently, cell death<sup>27</sup>.

Moreover, MIC values correlate with the previous findings by Romano *et al*<sup>28</sup> who reported that synthesised AgNPs using the halophilic strain *Halomonas* sp have potent antimicrobial activity and recorded comparable MIC endpoints against pathogens. The results demonstrated significant inhibition of AgNPs through

their surface characteristics and stability, enhancing bacterial membrane interaction and causing cellular disruption<sup>29</sup>.

Current results showed that *Hal*-AgNPs reduced viability in breast and cervical cancer cell lines, highlighting their potential as anticancer agents. The cytotoxicity is likely linked to apoptosis *via* mitochondrial pathways and elevated ROS levels induced by NP stress<sup>30</sup>. These findings support the use of halophilic archaea for NP synthesis, emphasising *Hal*-AgNPs' dual potential against multidrug-resistant bacteria and cancer.

The increasing demand for synthesised AgNPs in biomedical fields requires testing their toxicity to ensure biocompatibility in blood-containing medical devices. According to ASTM E2524-08 guidelines, a substance is haemocompatible if it causes <5 per cent haemolysis. The interaction between NPs and RBC membranes can cause membrane instability and haemoglobin leakage. In accordance, in this study the results showed that biogenically produced *Hal*-AgNPs exhibit low cytotoxicity toward RBCs, indicating high hemocompatibility. These findings align with research showing surface-engineered NPs' low haemolysis at similar concentrations<sup>31</sup>.

The differential cytotoxicity of *Haloferax* sp biosynthesised AgNPs (*Hal*-AgNPs) aligns with literature showing AgNP cytotoxicity occurs through oxidative stress and DNA damage *via* reactive oxygen species (ROS)<sup>32</sup>. This mechanism likely underpins the enhanced sensitivity of cancer cells (Mcf7, MDA-MB231, HELA) to *Hal*-AgNPs compared to non-cancerous Wi38 cells, given the former's higher metabolic rates and lower antioxidant defences. Further, the toxicity of AgNPs, as detailed by Akhtar *et al*<sup>33</sup>, involves silver ions (Ag<sup>+</sup>) released into the cytosol after endocytosis, disrupting cellular and metabolic cycles. HepG2 liver cancer cells showed higher sensitivity to AgNPs than Caco2 colon cancer cells. Cell-specific factors like metabolic rate and antioxidant defences influence responses to NP stress.

These interpretations align with observed trends; sensitivity was highest in Mcf7 and HELA cells, lower in MDA-MB231 cells, and significantly lower in the non-cancerous Wi38 line. This suggested that *Hal*-AgNPs may preferentially affect cells with reduced redox control or faster growth rates, typical of malignant cells, while sparing healthy cells. Such differential effects are significant for nanomedicine, suggesting targeted treatments that maximise efficacy

while minimising harm. The *Haloferax* sp biosynthesis method offers a green-chemistry approach yielding NPs for selective cancer cell targeting. However, comprehensive studies *in vivo* are needed to understand the long-term effects of *Hal*-AgNPs before clinical use. Exploring synergistic effects with chemotherapy and developing targeted delivery systems could enhance their therapeutic potential.

**Financial support & sponsorship:** The study received fund by the University of Jeddah, Jeddah, under Grant No. (UJ-23-DR-188).

**Conflicts of Interest:** None.

**Use of Artificial Intelligence (AI)-Assisted Technology for manuscript preparation:** The authors confirm that there was no use of AI-assisted technology for assisting in the writing of the manuscript and no images were manipulated using AI.

## References

1. Aberathna A, Satharasinghe DA, Jayaweera BPA, Manopriya S, Prathapasinghe GA, Liyanage JA, *et al*. Synthesis of phosphorus related nanoparticles by using microorganisms as an option for increasing bioavailability. *The Microbe* 2024; 3 : 100065.
2. Magdy G, Elattar RH, Abdel Salam RA, Hadad GM, El-Deen AK. Unlocking the power of nanohybrids: a critical review on carbon nanomaterial-functionalized silver nanoparticles for advanced antimicrobial applications. *Colloids Surf B Biointerfaces* 2025; 252 : 114678.
3. Danişman-Kalındemirtaş F, Kariper İ.Afşin, Hepokur C, Erdem-Kuruca S. Selective cytotoxicity of paclitaxel bonded silver nanoparticle on different cancer cells. *J Drug Deliv Sci Tech* 2021; 61 : 102265.
4. Hjartákær A, Weiderpass E, Bray F. Cancer mortality. In: Quah SR, editor. *International encyclopedia of public health*. Elsevier; 2025. p. 171-82.
5. Li J, Kuang X. Global cancer statistics of young adults and its changes in the past decade: Incidence and mortality from GLOBOCAN 2022. *Public Health* 2024; 237 : 336-43.
6. Meyer M, Fourie C, van der Merwe H, Botha H, Engelbrecht AM. Targeting treatment resistance in cervical cancer: a new avenue for senolytic therapies. *Adv Med Sci* 2025; 70 : 33-4.
7. Lin C, Huang X, Xue Y, Jiang S, Chen C, Liu Y, *et al*. Advances in medical devices using nanomaterials and nanotechnology: Innovation and regulatory science. *Bioact Mater* 2025; 48 : 353-69.
8. Sadeghi Hosnijeh M, Hosseini Tafreshi SA, Masoum S. Nanophycology, the merging of nanoscience into algal research: a review. *Ecotoxicol Environ Saf* 2024; 282 : 116727.
9. Xu L, Wang YY, Huang J, Chen CY, Wang ZX, Xie H. Silver nanoparticles: Synthesis, medical applications and biosafety. *Theranostics* 2020; 10 : 8996-9031.

10. Sorokin DY, Elcheninov AG, Merkel AY, Bale NJ, Sininghe-Damste J, Kublanov IV. Halapricum hydrolyticum sp. nov., a beta-1,3-glucan utilizing haloarchaeon from hypersaline lakes. *Syst Appl Microbiol* 2023; 46 : 126471.
11. Tag HM, Saddiq AA, Alkinani M, Hagagy N. Biosynthesis of silver nanoparticles using Haloferax sp NRS1: Image analysis, characterization, in vitro thrombolysis and cytotoxicity. *AMB Express* 2021; 11 : 75.
12. López-Ortega MA, Rodríguez-Hernández AI, Camacho-Ruiz RM, Córdova J, López-Cuellar MDR, Chavarria-Hernández N, et al. Physicochemical characterization and emulsifying properties of a novel exopolysaccharide produced by haloarchaeon Haloferax mucosum. *Int J Biol Macromol* 2020; 142 : 152-6.
13. Hagagy N, Saddiq AAN, Tag HM, Abdelgawad H, Selim S. Characterization of bioplastics produced by haloarchaeon Haloarcula sp strain NRS20 using cost-effective carbon sources. *Mater Res Express* 2021; 8 : 105404.
14. Espinel-Ingroff A, Canton E, Fothergill A, Ghannoum M, Johnson E, Jones RN, et al. Quality control guidelines for amphotericin b, Itraconazole, posaconazole, and voriconazole disk diffusion susceptibility tests with nonsupplemented Mueller-Hinton Agar (CLSI M51-A document) for nondermatophyte Filamentous Fungi. *J Clin Microbiol* 2011; 49 : 2568-71.
15. Hon KW, Zainal Abidin SA, Abas F, Othman I, Naidu R. Anti-cancer mechanisms of Diaryl pentanoid MS17 (1, 5-Bis (2-hydroxyphenyl)-1, 4-pentadiene-3-one) in human colon cancer cells: a proteomics approach. *Int J Mol Sci* 2024; 25 : 3503.
16. Patil S, Fernandes J, Tangasali R, Furtado I. Exploitation of haloferax alexandrinus for biogenic synthesis of silver nanoparticles antagonistic to human and lower mammalian pathogens. *J Clust Sci* 2014; 25 : 423-3.
17. Nabika H, Unoura K. Interaction between nanoparticles and cell membrane. In: Grumezescu A, editor. *Surface Chemistry of Nanobiomaterials*. William Andrew; Elsevier; 2016. p. 231-63.
18. Hamouda RA, Hussein MH, Elhadary AMA, Abuelmagd MA. Extruded polysaccharide/protein matrix from Arthrospira platensis cultures mediated silver nanoparticles biosynthesis and capping. *Appl Nanosci* 2020; 10 : 3839-55.
19. Thakar M, Trivedi P, Sindhav G. Sustainable biosynthesis of silver nanoparticles from gmelina arborea: photocatalytic, in vitro biological implications, and in silico analysis for microbial metalloproteins. *J Mol Liq* 2025; 422 : 126966.
20. Teh HY, Lam MK, Chai YH, Lim JW, Wong V-L, Tan IS, et al. Green synthesis of silver nanoparticles by algae: Advancements, challenges and sustainable prospects. *Materials Today Chem* 2024; 42 : 102389.
21. Székely-Szentmiklósi I, Rédei EM, Szabó ZI, Kovács B, Albert C, Gergely AL, et al. Microencapsulation by complex coacervation of lavender oil obtained by steam distillation at semi-industrial scale. *Foods* 2024; 13 : 2935.
22. Basu A, Vaskevich A, Chuntunov L. Glutathione self-assembles into a shell of hydrogen-bonded intermolecular aggregates on “naked” silver nanoparticles. *J Phys Chem B* 2021; 125 : 895-906.
23. Abdel Rahim K, Mahmoud SY, Ali AM, Almaary KS, Mustafa AE, Husseiny SM. Extracellular biosynthesis of silver nanoparticles using Rhizopus stolonifer. *Saudi J Biol Sci* 2017; 24 : 208-16.
24. Sheng Y, Narayanan M, Basha S, Elfasakhany A, Brindhadevi K, Xia C, et al. In vitro and in vivo efficacy of green synthesized AgNPs against Gram negative and Gram positive bacterial pathogens. *Process Biochem* 2022; 112 : 241-7.
25. Abbaszadegan A, Ghahramani Y, Gholami A, Hemmateenejad B, Dorostkar S, Nabavizadeh M, et al. The effect of charge at the surface of silver nanoparticles on antimicrobial activity against gram-positive and gram-negative bacteria: A preliminary study. *J Nanomater* 2015; 2015.
26. John MS, Nagoth JA, Ramasamy KP, Mancini A, Giuli G, Natalello A, et al. Synthesis of bioactive silver nanoparticles by a pseudomonas strain associated with the Antarctic psychrophilic protozoon Euplotes focardii. *Mar Drugs* 2020; 18 : 38.
27. Nguyen DH, Lee JS, Park KD, Ching YC, Nguyen XT, Phan VH, et al. Green silver nanoparticles formed by phyllanthus urinaria, pouzolzia zeylanica, and scoparia dulcis leaf extracts and the antifungal activity. *Nanomaterials (Basel)* 2020; 10 : 542.
28. Romano I, Vitiello G, Gallucci N, Di Girolamo R, Cattaneo A, Poli A, et al. Extremophilic microorganisms for the green synthesis of antibacterial nanoparticles. *Microorganisms* 2022; 10 : 1885.
29. Modi SK, Gaur S, Sengupta M, Singh MS. Mechanistic insights into nanoparticle surface-bacterial membrane interactions in overcoming antibiotic resistance. *Front Microbiol* 2023; 14 : 1135579.
30. Li B, Zhang T, Tang M. Toxicity mechanism of nanomaterials: Focus on endoplasmic reticulum stress. *Sci Total Environ* 2022; 834 : 155417.
31. Kumar S, Jha I, Mogha NK, Venkatesu P. Biocompatibility of surface-modified gold nanoparticles towards red blood cells and haemoglobin. *Appl Surf Sci* 2020; 512 : 145573.
32. Amalin Sobi M, Bindhu MR, Usha D, Rajagopal R, Alfarhan A, Arokiyaraj S, et al. Molecular insights into quercetin-enhanced crystalline silver nanoparticles: Implications for breast cancer cell cytotoxicity and antibacterial action in *Kylinella nemoralis*. *J Cryst Growth* 2024; 637-38.
33. Akhtar MJ, Ahamed M, Alhadlaq H. A selective toxicity of Pt-coated Au nanoparticles in cancerous MCF-7 cells over non-cancerous HUVE cells. *J King Saud Univ Sci* 2023; 35 : 102583.